arXiv:cond-mat/9702064v1 6 Feb 1997

C-axis Transport in Bilayer Cuprates and Relation to Pseudogap

W. C. Wu[a], W. A. Atkinson[b], and J. P. Carbotte[a]
[a] *Department of Physics and Astronomy, McMaster University, Hamilton, Ontario, Canada L8S 4M1*
[b] *Department of Physics, Indiana University, Swain Hall W 117, Bloomington, IN 47405*
(February 1, 2008)

We consider the effect of interband transitions on the c-axis conductivity, DC resistivity, and thermal conductivity in a plane-chain bilayer model of a cuprate. The relation between the c-axis resistivity and thermal conductivity is governed by the Wiedemann-Franz law. When the perpendicular hopping matrix element between chain and plane ($t_\perp$) is small, the c-axis DC resistivity shows a characteristic upturn as the temperature is lowered and the infrared conductivity develops a pseudogap. As $t_\perp$ is increased, intraband transitions start to dominate and a more conventional response is obtained. Analytical results for a simple plane-plane bilayer are also given, including the frequency sum rule of the optical conductivity.

PACS numbers: 74.80.Dm, 78.30.-j, 74.25.Jb, 74.72.-h

I. INTRODUCTION

In a previous paper [1], we derived expressions for, and computed, the normal-state optical conductivity for a system of two layers per unit cell coupled through a hopping matrix element $t_\perp$ which introduces the third dimension. In addition to the usual intraband terms, which give a Drude-like response, interband transitions are now possible and these have quite a different temperature and frequency dependence. It was found that for sufficiently small values of $t_\perp$, the interband terms, which are of order $t_\perp^2$, dominate over the intraband contribution which goes like $t_\perp^4$ for the c-axis. In this limit, the c-axis response can be very different from Drude. In general, the interband transitions occur at energies which extend over the entire band width and structure in the c-axis conductivity can be directly related to certain features of the band structure. For the particular case of a CuO_2 tetragonal plane and a set of CuO chains [2–4], it was found that the normal-state c-axis response can develop a gap or pseudogap at low ω depending on the details of the two Fermi surfaces involved.

Estimated values of $t_\perp$ have been provided by Zha, Cooper and Pines [5]. They give $t_\perp \sim 3.0$meV for underdoped $YBCO_{6.68}$ and 30 to 40meV for optimally doped $YBCO_{6.93}$. These estimates are much larger than for the more anisotropic compounds such as $Bi_2Sr_2CaCu_2O_8$ where $t_\perp$ is perhaps as small as 0.1meV. It is clear from these estimates that underdoped YBCO could be in the interband dominated regime and show a pseudogap response while optimally doped and overdoped YBCO would show a more usual Drude-like c-axis response as in this case, intraband transitions would dominate over interband.

In this paper, we wish to consider the c-axis transport and study the effect of interband transitions on its temperature dependence. For fully oxygenated YBCO, the resistivity $\rho(T)$ in the c-axis [6–13] is found to exhibit metallic behavior and show a nearly linear temperature dependence which follows that in the a-b plane but, of course, has a very different magnitude with ρ_c/ρ_{ab} of order 30 to 70. On the other hand, for deoxygenated underdoped samples corresponding to small $t_\perp$, the situation is very different and $\rho_c(T)$ shows a semiconductivity-like behavior [8,10–13] at low temperatures ($d\rho_c/dT < 0$), while at high temperatures, the linear behavior is retained. The ratio ρ_c/ρ_{ab} is however very much larger than that observed in the fully oxygenated case with ρ_c/ρ_{ab} at $T = 100K$ of order 10^3. Estimates of c-axis mean free paths based on such large values of ρ_c lead to values that are of the order and even less than the c-axis spacing between planes. This realization has led some to suggest that conventional three dimensional Bloch transport breaks down and that c-axis transport proceeds through an incoherent mechanism due to confinement coming from the highly two dimensional nature of the electronic states. Here we consider that the interband transitions begin to dominate when $t_\perp$ is small. This effect has its origin in the fact that YBCO has several atoms per unit cell. In the real situation, there are two copper-oxygen planes and one set of chains. For simplicity, here we will consider only a plane-chain model which is believed to capture some of the qualitative features of the interband transitions.

In Sec. II, we establish the Kubo formula for the AC infrared conductivity in the case of a plane-chain model coupled through a transverse hopping matrix element $t_\perp$ in tight binding. The usual formula becomes a trace over the two bands and the electromagnetic vertices are now a 2×2 matrix with off-diagonal elements related to the derivatives of the Hamiltonian matrix. The resulting formula easily separates into interband and intraband parts. In Sec. III, analytic results for the infrared conductivity and the DC resistivity are presented for the case of infinite bands with minimum energy difference between them of Δ. One band is taken to have a one-dimensional character and the other two-dimensional. The role of the pseudogap Δ in these quantities is made clear. In Sec. IV, the thermal conductivity is considered and the Wiedemann-Franz law is established for the c-axis including interband as well as intraband contributions. In Sec. V, we treat the case of a plane-plane bilayer

which is important because simpler analytic results can be obtained including for the conductivity sum rule. In Sec. VI, tight-binding bands are introduced and numerical results presented for this more complicated case which does not yield to any analytic analysis but includes such effects as the Van Hove singularity in the electronic density of states. Nevertheless the results show no qualitative difference with those presented in previous sections based on simplified infinite bands. A short conclusion can be found in Sec. VII.

II. FORMALISM

We start with the Hamiltonian for a plane-chain bilayer coupled through a transverse matrix element $t_\perp$. In a matrix notation, we start with creation $C_{\mathbf{k}}^\dagger$ and annihilation $C_{\mathbf{k}}$ operators

$$C_{\mathbf{k}}^\dagger = \left(c_{1\mathbf{k}}^\dagger, c_{2\mathbf{k}}^\dagger\right) \quad ; \qquad C_{\mathbf{k}} = \begin{pmatrix} c_{1\mathbf{k}} \\ c_{2\mathbf{k}} \end{pmatrix}, \tag{1}$$

with $c_{1\mathbf{k}}^\dagger (c_{2\mathbf{k}}^\dagger)$ creating an electron in the state of momentum $\mathbf{k}$ in layer 1 (2), respectively. The Hamiltonian operator H_0 is

$$H_0 = \sum_{\mathbf{k}} C_{\mathbf{k}}^\dagger h(\mathbf{k}) C_{\mathbf{k}}, \tag{2}$$

where the Hamiltonian matrix

$$h(\mathbf{k}) = \begin{pmatrix} \xi_1(\mathbf{k}) & t(k_z) \\ t(k_z) & \xi_2(\mathbf{k}) \end{pmatrix}, \tag{3}$$

with

$$\xi_1(\mathbf{k}) = \frac{\hbar^2}{2m}(k_x^2 + k_y^2) - \mu + \Delta, \tag{4a}$$

$$\xi_2(\mathbf{k}) = \frac{\hbar^2}{2m} k_y^2 - \mu, \tag{4b}$$

for the plane and chain respectively and

$$t(k_z) = -2t_\perp \cos\left(\frac{k_z d}{2}\right) \tag{5}$$

with d the distance between chain and plane in the z-direction and $t_\perp$ the coupling strength. In (4), μ is the chemical potential, Δ is the minimum energy difference between the two bands and is responsible for the pseudogap in the c-axis response, $\hbar$ is the Planck's constant over 2π and m is the bare electron mass.

When a vector potential $\mathbf{A}(\mathbf{q})$ is applied to the system, the Hamiltonian changes to [14,15]

$$H = H_0 - \frac{e}{2mc}\mathbf{p}\cdot\mathbf{A} \tag{6}$$

to the lowest order in $\mathbf{A}$, with the vector

$$\mathbf{p} = \frac{m}{\hbar}\sum_{\mathbf{k}} C_{\mathbf{k}}^\dagger \frac{\partial h(\mathbf{k})}{\partial \mathbf{k}} C_{\mathbf{k}}. \tag{7}$$

Using the Kubo formula for the current-current correlation function, this leads directly to a real-part conductivity in the c-axis of the form ($\mathrm{Re}\sigma_{zz}(\omega) \equiv \sigma_c(\omega)$)

$$\sigma_c(\omega) = e^2 \frac{1}{\Omega}\sum_{\mathbf{k}} \int_{-\infty}^{\infty} \frac{dx}{2\pi}\, \frac{f(x) - f(x+\hbar\omega)}{\omega}$$
$$\times \mathrm{Tr}[A(\mathbf{k},x)\gamma_z(\mathbf{k},\mathbf{k})A(\mathbf{k},x+\hbar\omega)\gamma_z(\mathbf{k},\mathbf{k})], \tag{8}$$

where "Tr" is a trace, $A(\mathbf{k},\omega)$ is the spectral function matrix, and γ_z is the associated c-axis electromagnetic vertex function matrix given by

$$\gamma_z = \frac{1}{\hbar}\frac{\partial h(\mathbf{k})}{\partial k_z}. \tag{9}$$

The "trace" operator in (8) allows one to work in any frame which is convenient. We will choose a frame in which the Green's function (and hence the spectral function) matrix is diagonal. Consequently, one obtains (following Ref. [1])

$$\sigma_c(\omega) = e^2 \frac{1}{\Omega}\sum_{\mathbf{k}} \int_{-\infty}^{\infty} \frac{dx}{2\pi}\, \frac{f(x) - f(x+\hbar\omega)}{\omega} \tag{10}$$
$$\times \left[\left(A_{11}A'_{11} + A_{22}A'_{22}\right)\gamma_{11}^2 + \left(A_{11}A'_{22} + A_{22}A'_{11}\right)\gamma_{12}^2\right],$$

where $A_{ii} \equiv A_{ii}(\mathbf{k},x)$ and $A'_{ii} \equiv A_{ii}(\mathbf{k},x+\hbar\omega)$ and the vertices

$$\gamma_{11} = v_\perp \left(\frac{2t}{\epsilon_+ - \epsilon_-}\right)$$
$$\gamma_{12} = v_\perp \left(\frac{\xi_1 - \xi_2}{\epsilon_+ - \epsilon_-}\right), \tag{11}$$

with $v_\perp \equiv 1/\hbar\partial t/\partial k_z = t_\perp d/\hbar \sin(k_z d/2)$. More explicitly, in the normal state, the spectral functions

$$A_{ii}(\mathbf{k},x) = \frac{2\Gamma_i}{(x-\epsilon_i)^2 + \Gamma_i^2}, \tag{12}$$

where $\epsilon_1 \equiv \epsilon_+$, $\epsilon_2 \equiv \epsilon_-$, and Γ_i is the total scattering rate in band i. A realistic model for the high-T_c oxides is that the scattering rate is dominated by the inelastic scattering with Γ linear in temperature T. The energies

$$\epsilon_\pm = \frac{\xi_1 + \xi_2}{2} \pm \sqrt{\left(\frac{\xi_1 - \xi_2}{2}\right)^2 + t^2} \tag{13}$$

are the two renormalized bands.

It is clear from the form of Eq. (10) that with the initial and final states in the same band, the first term corresponds to the *intraband* contribution and the second term corresponds to the *interband* contribution with the initial and final states in different bands. From the form of the vertices given in (11), one sees immediately that the interband contribution ($\sim t_\perp^2$) dominates the intraband contribution ($\sim t_\perp^4$) in the small-$t_\perp$ limit. For simplicity, we will assume the scattering rate $\Gamma_1 = \Gamma_2 \equiv \Gamma$ in all our calculations.

III. CONDUCTIVITY AND DC RESISTIVITY

Substituting (4), (11), and (12) into (10), the intraband contribution for the c-axis conductivity is explicitly given by

$$\sigma_c^{\rm intra}(\omega) = e^2 \frac{1}{\Omega} \sum_{\mathbf{k}} v_\perp^2 \left(\frac{2t}{\epsilon_+ - \epsilon_-} \right)^2 \int_{-\infty}^{\infty} \frac{dx}{2\pi} \frac{f(x) - f(x+\hbar\omega)}{\omega} \left[\frac{2\Gamma}{(x-\epsilon_+)^2 + \Gamma^2} \frac{2\Gamma}{(x+\hbar\omega-\epsilon_+)^2 + \Gamma^2} + \frac{2\Gamma}{(x-\epsilon_-)^2 + \Gamma^2} \frac{2\Gamma}{(x+\hbar\omega-\epsilon_-)^2 + \Gamma^2} \right]. \tag{14}$$

To reduce (14) further, we first replace the momentum $\mathbf{k}$-sum by an integral

$$\frac{1}{\Omega} \sum_{\mathbf{k}} \rightarrow \int_{-\frac{\pi}{d}}^{\frac{\pi}{d}} \frac{dk_z}{2\pi} \int_{-\infty}^{\infty} N(0) d\epsilon, \tag{15}$$

where ϵ can be either ϵ_+ or ϵ_- and a constant "2D" density of states per spin at Fermi level $N(0) \equiv m/2\pi\hbar^2$ is assumed (in the small-$t_\perp$ limit). Secondly, we replace the factor $\epsilon_+ - \epsilon_-$ in (14) by the (constant) band gap Δ. This approximation is quite good and has only a small effect on the final results. As a result of the above simplification, the k_z dependence in the integrand comes in only through $t(k_z)$ and $v_\perp(k_z)$ which can be easily carried out to get $\int_{-\frac{\pi}{d}}^{\frac{\pi}{d}} \frac{dk_z}{2\pi} v_\perp^2 t^2 = t_\perp^4 d/2\hbar^2$. Consequently, (14) reduces to

$$\sigma_c^{\rm intra}(\omega) = \frac{8e^2 t_\perp^2 N(0) d}{\pi\hbar^2} \left(\frac{t_\perp}{\Delta} \right)^2 \int_{-\infty}^{\infty} d\epsilon \int_{-\infty}^{\infty} dx \frac{f(x) - f(x+\hbar\omega)}{\omega} \frac{\Gamma}{(x-\epsilon)^2 + \Gamma^2} \frac{\Gamma}{(x+\hbar\omega-\epsilon)^2 + \Gamma^2}, \tag{16}$$

where the two bands give the *same* contributions for the intraband part of the c-axis conductivity. Furthermore, with the aid of

$$\int_{-\infty}^{\infty} d\epsilon \frac{\Gamma}{(x-\epsilon)^2 + \Gamma^2} \frac{\Gamma}{(x+\hbar\omega-\epsilon)^2 + \Gamma^2} = \pi \frac{2\Gamma}{(\hbar\omega)^2 + 4\Gamma^2} \tag{17}$$

and

$$\int_{-\infty}^{\infty} dx \frac{f(x) - f(x+\hbar\omega)}{\omega} = \hbar, \tag{18}$$

one immediately obtains the final result

$$\sigma_c^{\rm intra}(\omega) = \frac{8e^2 t_\perp^2 N(0) d}{\hbar} \left(\frac{t_\perp}{\Delta} \right)^2 \frac{2\Gamma}{(\hbar\omega)^2 + 4\Gamma^2} \tag{19}$$

which is nothing but the "Drude" theory.

In analogy to (14), the interband contribution of the c-axis conductivity is given by

$$\sigma_c^{\rm inter}(\omega) = e^2 \frac{1}{\Omega} \sum_{\mathbf{k}} v_\perp^2 \int_{-\infty}^{\infty} \frac{dx}{2\pi} \frac{f(x) - f(x+\hbar\omega)}{\omega} \left[\frac{2\Gamma}{(x-\epsilon_+)^2 + \Gamma^2} \frac{2\Gamma}{(x+\hbar\omega-\epsilon_-)^2 + \Gamma^2} + \frac{2\Gamma}{(x-\epsilon_-)^2 + \Gamma^2} \frac{2\Gamma}{(x+\hbar\omega-\epsilon_+)^2 + \Gamma^2} \right], \tag{20}$$

where we note that the second term dominates when $\omega \geq 0$ (because $\epsilon_+ \geq \epsilon_-$). To calculate (20), the simplification (15) used for the calculations of intraband part is no longer valid because now the two bands come in together and the correlation and difference between these two bands are certainly important. One therefore needs instead to replace the momentum $\mathbf{k}$-sum in (20) by the integral

$$\frac{1}{\Omega} \sum_{\mathbf{k}} \rightarrow \int_{-\frac{\pi}{d}}^{\frac{\pi}{d}} \frac{dk_z}{2\pi} \int_{-\infty}^{\infty} \frac{dk_x}{2\pi} \int_{-\infty}^{\infty} \frac{dk_y}{2\pi}. \tag{21}$$

To simplify the calculation, we will approximate $\epsilon_+ = \xi_1$ and $\epsilon_- = \xi_2$ in the small-$t_\perp$ limit (see (13)). This simplification was not done in Ref. [1] where the $\mathbf{k}$-sum is carried out directly by numerical integration over the first Brillouin zone. Note that this means that they are effectively including the Van Hove singularity in the electronic density of states which we have taken as constant. The integration over k_z can be carried out first to be $\int_{-\pi/d}^{\pi/d} \frac{dk_z}{2\pi} v_\perp^2 = t_\perp^2 d/2\hbar^2$. Moreover, with

$$\int_{-\infty}^{\infty} dk_x \frac{1}{(A - \hbar^2 k_x^2/2m)^2 + \Gamma^2} = \frac{\sqrt{m}\pi}{\hbar} \frac{1}{\sqrt{A^2+\Gamma^2}\sqrt{\sqrt{A^2+\Gamma^2} - A}}, \tag{22}$$

$\sigma_c^{\rm inter}$ in (20) can be reduced to (changing the variable $dk_y \rightarrow d\epsilon_- = d\xi_2$)

$$\sigma_c^{\rm inter}(\omega) = \frac{e^2 t_\perp^2 N(0) d}{\hbar^2} \sqrt{2}\pi \times \int_{-\infty}^{\infty} dx \frac{f(x) - f(x+\hbar\omega)}{\omega} \int_{-\mu}^{\infty} \frac{d\epsilon_-}{\sqrt{\epsilon_- + \mu}} \left[\frac{\Gamma}{\left[(x+\hbar\omega-\epsilon_-)^2 + \Gamma^2\right] \sqrt{(x-\epsilon_--\Delta)^2 + \Gamma^2}} \times \frac{\Gamma}{\sqrt{\sqrt{(x-\epsilon_--\Delta)^2+\Gamma^2} - (x-\epsilon_--\Delta)}} + \frac{\Gamma}{\left[(x-\epsilon_-)^2 + \Gamma^2\right] \sqrt{(x-\epsilon_-+\hbar\omega-\Delta)^2 + \Gamma^2}} \times \frac{\Gamma}{\sqrt{\sqrt{(x-\epsilon_-+\hbar\omega-\Delta)^2+\Gamma^2} - (x-\epsilon_-+\hbar\omega-\Delta)}} \right], \tag{23}$$

with $N(0) \equiv m/2\pi\hbar^2$. A crucial point seen in (23) is that the chemical potential (or filling) plays a role in the interband transition, as expected.

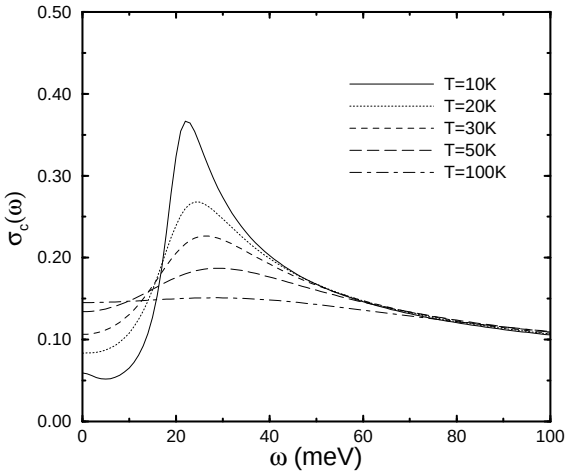

FIG. 1. c-axis conductivity as a function of photon energy for a plane-chain bilayer at different temperatures with a small $t_\perp = 2$meV. The minimum energy difference between the two bands for a given $\mathbf{k}$ in the first 2D Brillouin zone is $\Delta = 20$meV.

Based on the intraband contribution given by the analytical result (19) and the interband contribution given by the numerical calculations of (23), we have plotted the c-axis conductivity in Fig. 1 for various temperatures at fixed $t_\perp = 2$meV and in Fig. 2 for fixed temperature $T = 30K$ at various $t_\perp$. We have used the same parameters: $\Delta = 20$meV, $\mu = 500$meV, and Γ is taken to be linear in temperature with $\Gamma = 20$meV at $T = 100K$ throughout this paper unless specified. This is motivated by the fact that the inelastic scattering rate is observed to be large and of the order of T_c [5] at the superconducting critical temperature (T_c) and varying almost linearly with temperature T. Also the evidence is that good samples show little or no residual resistivity and are therefore in the pure limit (there is no residual elastic scattering). One sees in Fig. 1 that a pseudogap can develop at low temperatures for small $t_\perp$ (in which case the interband transitions dominate). At higher temperatures, the pseudogap is invisible due to the stronger inelastic damping effect.

While in this paper we have made simplifications and approximations to the band structure, for example, we used the infinite-band approximation (15) with constant density of states evaluated at the Fermi energy and taken it out of the integral, this was not done in Ref. [1] where the full sum over the Brillouin zone which includes a Van Hove singularity in the electronic density of states was performed numerically and the effect of $t_\perp$ on the bands (see Eq. (13)) was fully included. We observe however that there are no qualitative differences between the results of Fig. 1 and those of Fig. 2 in Ref. [1]. The results of Ref. [1] do show some structure at higher energy which reflects special features of the plane-chain tight binding bands used in that study but not in this work, but these are small and we can safely proceed with a discussion of the DC resistivity using the simplified infinite band structure of Eq. (4) which allows the required numerical work to be greatly simplified.

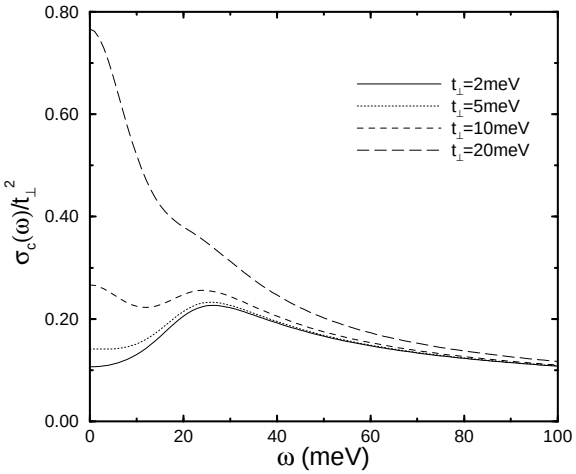

FIG. 2. c-axis conductivity for a plane-chain bilayer for different values of coupling $t_\perp$ at $T = 30K$ with minimum energy between the two bands equal to $\Delta = 20$meV.

Fig. 2 shows that by increasing strength of $t_\perp$, the pseudogap can disappear. For clarity of presentation, all intensities in Fig. 2 have been divided by $t_\perp^2$. This leads to a nearly constant interband contribution plus a intraband (Drude-like) contribution proportional to $t_\perp^2$ which increases with increasing values of $t_\perp$. In the case of larger $t_\perp$, the intraband transition and hence the Drude-like behavior becomes dominant (long dashed curve with $t_\perp = 20$meV) over the smaller interband contribution which now appears above ~ 20meV. We stress and it is clear from the figures that the value of the real part of the conductivity at higher energies is entirely due to interband contributions since in our model the Drude contribution is sharply peaked about $\omega = 0$ on the energy scale of 150 to 200 meV.

We have also plotted in Figs. 3 and 4 the c-axis DC resistivity for the plane-chain bilayer normalized to its value at $300K$. As shown in Fig. 3, when $t_\perp$ is small the c-axis DC resistivity shows a characteristic upturn as the temperature is lowered such as those observed in semiconductors. This characterizes the importance of the interband transition. A "pseudogap" in the joint density of states (interband contribution) suppresses the interlayer hopping and gives rise to the semiconductor-like $\rho_c(T)$. When $t_\perp$ is increased, intraband transitions start to dominate and a more conventional response (linear in T) is obtained. A similar plot as given in Fig. 3 given in Fig. 4 shows that when the pseudogap is reduced (or relatively the $t_\perp$ is larger), the upturn feature becomes much less dramatic.

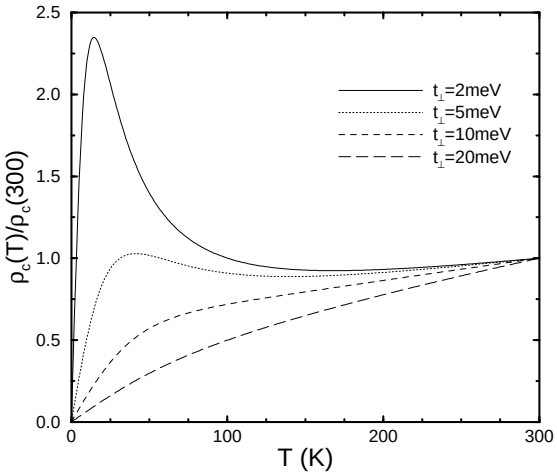

FIG. 3. Temperature-dependent c-axis DC resistivity for a plane-chain bilayer for different values of $t_\perp$. The minimum energy between the two bands is $\Delta = 20$meV.

To gain more insight into the relationship between the c-axis conductivity and DC resistivity in a plane-chain bilayer, we derive in the following some analytic results under certain limits. When temperature is not too high and hence Γ is sufficiently small (it is assumed to vary linearly with T), one can approximate

$$\frac{\Gamma}{(x-\epsilon_-)^2+\Gamma^2} \to \pi\delta(\epsilon_- - x) \tag{24}$$

in the second term of (23) which one recalls dominates in the case of $\omega > 0$ which is of interest. Moreover, due to the behavior of the Fermi distribution functions, the integration over x in (23) contributes mainly from $x = -\hbar\omega - k_BT$ to $x = k_BT$. One thus can replace $\int_{-\mu}^{\infty} d\epsilon_-$ by $\int_{-\infty}^{\infty} d\epsilon_-$ assuming $\hbar\omega \ll \mu$. Consequently, after the integration over $d\epsilon_-$, the second term of (23) reduces to

$$\frac{e^2t_\perp^2 N(0)d}{\hbar^2}\sqrt{2}\pi^2 \int_{-\infty}^{\infty} dx\ \frac{f(x)-f(x+\hbar\omega)}{\omega}\frac{1}{\sqrt{x+\mu}} \frac{\Gamma}{\sqrt{(\hbar\omega-\Delta)^2+\Gamma^2}\sqrt{\sqrt{(\hbar\omega-\Delta)^2+\Gamma^2}-(\hbar\omega-\Delta)}}. \tag{25}$$

Eq. (25) allows one to discuss some analytic results of $\sigma_c^{\rm inter}$ (and hence σ_c).

For high frequencies ($\hbar\omega - \Delta \gg \Gamma, k_BT$), one can approximate $\int_{-\infty}^{\infty} dx\,[f(x)-f(x+\hbar\omega)]$ by $\int_{-\hbar\omega}^{0} dx$, and, as a result, the associated x-integration can be performed easily to be

$$\int_{-\hbar\omega}^{0} dx\ \frac{1}{\sqrt{x+\mu}} = 2(\sqrt{\mu}-\sqrt{\mu-\omega}). \tag{26}$$

Next by expanding

$$\sqrt{\sqrt{(\hbar\omega-\Delta)^2+\Gamma^2}-(\hbar\omega-\Delta)} \simeq \frac{\Gamma}{\sqrt{2(\hbar\omega-\Delta)}}, \tag{27}$$

one obtains following (25)

$$\sigma_c^{\rm inter} \ \sim\ t_\perp^2 \frac{\sqrt{\mu}-\sqrt{\mu-\omega}}{\omega\sqrt{\hbar\omega-\Delta}}, \tag{28}$$

which is *independent* of Γ (or T) and is proportional to $\omega^{-\frac{1}{2}}$ when $\mu \gg \omega \gg \Delta$.

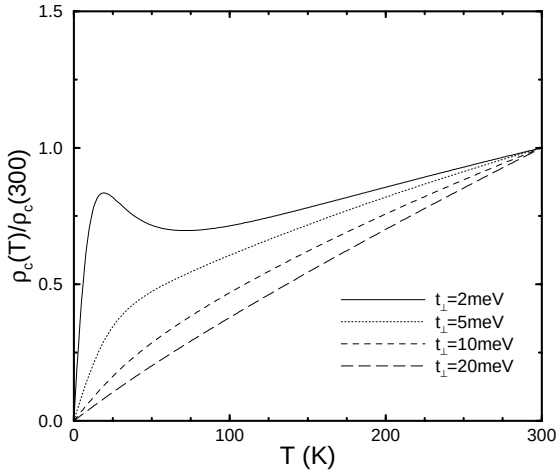

FIG. 4. Similar plot as Fig. 3, but for $\Delta = 10$meV.

For low frequencies ($\hbar\omega \ll \Delta$), one has $[f(x)-f(x+\hbar\omega)]/\omega \to \hbar\delta(x)$, and following (25)

$$\sigma_c^{\rm inter}(\omega) \ \sim\ t_\perp^2\mu^{-\frac{1}{2}} \times\frac{\Gamma}{\sqrt{(\hbar\omega-\Delta)^2+\Gamma^2}\sqrt{\sqrt{(\hbar\omega-\Delta)^2+\Gamma^2}-(\hbar\omega-\Delta)}}, \tag{29}$$

which is proportional to Γ when $\Gamma \ll \Delta$ and is proportional to $\Gamma^{-\frac{1}{2}}$ when $\Gamma \gg \Delta$. From the result (29) and (19) at $\omega = 0$, one can also get an expression for the DC resistivity ($\rho_c(T)$) for the plane-chain bilayer, which is then given by

$$\rho_c(T) \ \sim\ t_\perp^{-2}\Gamma \times\left[\left(\frac{t_\perp}{\Delta}\right)^2+\frac{\pi^2}{\sqrt{8}}\frac{\Gamma^2}{\sqrt{\mu}\sqrt{\Delta^2+\Gamma^2}\sqrt{\sqrt{\Delta^2+\Gamma^2}+\Delta}}\right]^{-1}. \tag{30}$$

It is clear from (30) that for $t_\perp \ll \Delta$ the first term in the square bracket is small and becomes important only when the second one is also small. For Γ small,

$$\rho_c(T) \ \sim\ t_\perp^{-2}\Gamma\left[\left(\frac{t_\perp}{\Delta}\right)^2+\frac{\pi^2}{4}\frac{\Gamma^2}{\sqrt{\mu\Delta^3}}\right]^{-1}, \tag{31}$$

the Drude contribution to the c-axis resistivity $\rho_c(T)$ goes like Γ while the interband contribution on its own has the inverse dependence and goes like Γ^{-1}. This is the physics underlying the upturn in the resistivity of Figs. 3 and 4 as T is lowered and is also the reason the pseudogap forms as seen in Fig. 1. The two effects are intimately connected in our theory.

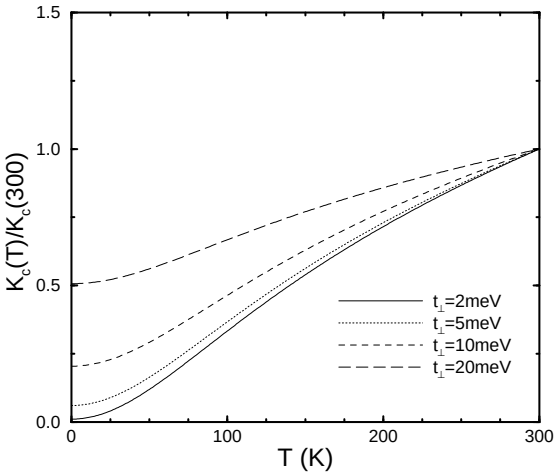

FIG. 5. Temperature-dependent c-axis thermal conductivity for a plane-chain bilayer for different values of $t_\perp$.

IV. THERMAL CONDUCTIVITY

In analogy to (8) for the c-axis optical conductivity, one can derive the c-axis thermal conductivity in terms of the Kubo formalism [16,17]

$$K_c(T) = \frac{1}{T\Omega}\sum_{\mathbf{k}}\int_{-\infty}^{\infty}\frac{dx}{2\pi}\,x^2\frac{\partial f(x)}{\partial x} \times \mathrm{Tr}[A(\mathbf{k},x)\gamma_z(\mathbf{k},\mathbf{k})A(\mathbf{k},x)\gamma_z(\mathbf{k},\mathbf{k})], \tag{32}$$

calculated at $\omega = 0$. Here $f(x)$ is the Fermi distribution function, $A(\mathbf{k},x)$ is the spectral function matrix, and $\gamma_z(\mathbf{k},\mathbf{k})$ is exactly the vertex function matrix for calculating the current-current correlation function given in (9). As we have done in (10) for the optical conductivity, due to the trace operator, one can work in a frame in which the Green's function is diagonal. This will lead to the fact that the c-axis thermal conductivity can be separated into intraband and interband contributions. However, this is not needed since we can establish that the c-axis thermal conductivity obeys the Wiedemann-Franz law. Due to the fact that the main contribution to integration over x for both (32) and (8) at $\omega = 0$ comes from the small region around $x = 0$, the x-dependence inside the trace for both (32) and (8) is removed. One easily finds by comparison that the ratio of the c-axis thermal conductivity to the c-axis DC electrical conductivity is

$$\frac{K_c}{\sigma_c(\omega=0)} = \frac{1}{T}\int_{-\infty}^{\infty}dx\;x^2\frac{\partial f(x)}{\partial x}\Big/e^2\int_{-\infty}^{\infty}dx\;\frac{\partial f(x)}{\partial x} = \left(\frac{k_B}{e}\right)^2 T\int_{-\infty}^{\infty}dy\;2y^2\mathrm{sech}^2 y = \frac{\pi^2}{3}\left(\frac{k_B}{e}\right)^2 T. \tag{33}$$

The above result is simply the Wiedemann-Franz law.

Using (30) with (33), one obtains (recall $\Gamma \sim T$)

$$K_c(T) \;\sim\; t_\perp^2 \times\left[\left(\frac{t_\perp}{\Delta}\right)^2 + \frac{\pi^2}{\sqrt{8}}\frac{\Gamma^2}{\sqrt{\mu}\sqrt{\Delta^2+\Gamma^2}\sqrt{\sqrt{\Delta^2+\Gamma^2}+\Delta}}\right], \tag{34}$$

and for small Γ (using (31))

$$K_c(T) \;\sim\; t_\perp^2\left[\left(\frac{t_\perp}{\Delta}\right)^2 + \frac{\pi^2}{4}\frac{\Gamma^2}{\sqrt{\mu\Delta^3}}\right]. \tag{35}$$

We have plotted $K_c(T)$ normalized to its value at $300K$ using (34) in Fig. 5. For small $t_\perp$, the significant depression of $K_c(T)$ at low temperature characterizes the importance of the interband transition in which case one will also see the depression of optical conductivity and the upturn of the DC resistivity associated with pseudogaps.

V. PLANE-PLANE BILAYER

Even simpler analytic results, which shed further light on the physics of our model can be obtained for a plane-plane bilayer in which the two uncoupled bands are given by (4) with ξ_2 now replaced by $\xi_2 = \frac{\hbar^2}{2m}(k_x^2+k_y^2)-\mu$. In this case, one can also have analytical results for the interband part of the c-axis conductivity

$$\sigma_c^{\mathrm{inter}}(\omega) = \frac{e^2t_\perp^2N(0)d}{\hbar}\left[\frac{2\Gamma}{(\hbar\omega+\Delta)^2+4\Gamma^2} + \frac{2\Gamma}{(\hbar\omega-\Delta)^2+4\Gamma^2}\right]. \tag{36}$$

The result (36) for $\sigma_c^{\mathrm{inter}}$ for the plane-plane bilayer leads to a peak feature at $\omega = \Delta$ but is otherwise similar to the results given by (25) (or more generally (23)) for a plane-chain bilayer. The simple analytic expression (36) thus helps gain physical insight into the c-axis transport properties.

A. Conductivity

The total c-axis conductivity given by the sum of (19) and (36) will be

$$\sigma_c(\omega) = \sigma_c^{\mathrm{intra}}(\omega)+\sigma_c^{\mathrm{inter}}(\omega) = \frac{e^2t_\perp^2N(0)d}{\hbar} \times\left[\left(\frac{2t_\perp}{\Delta}\right)^2\frac{4\Gamma}{(\hbar\omega)^2+4\Gamma^2} + \left(\frac{2\Gamma}{(\hbar\omega+\Delta)^2+4\Gamma^2}+\frac{2\Gamma}{(\hbar\omega-\Delta)^2+4\Gamma^2}\right)\right]. \tag{37}$$

Some features are:

- $\sigma_c^{\mathrm{intra}} \propto t_\perp^4$, $\sigma_c^{\mathrm{inter}} \propto t_\perp^2$, and the relative intensity $\sigma_c^{\mathrm{intra}}/\sigma_c^{\mathrm{inter}} \propto t_\perp^2/\Delta^2$.

- When $\omega \to 0$ and T (or Γ) is small, $\sigma_c^{\rm intra} \sim \Gamma^{-1} \sim T^{-1}$ (Drude like), while $\sigma_c^{\rm inter} \sim \Gamma \sim T$ (non-Drude like).
- The high-frequency tail of $\sigma_c(\omega)$ goes as ω^{-2} and decays very fast.
- The peak at $\omega = \Delta$ corresponds to the pseudogap and by changing the ratio of $t_\perp$ to Δ, the pseudogap can disappear.

B. Frequency Sum Rule

Because of

$$\int_0^\infty d\omega \frac{4\Gamma}{(\hbar\omega)^2+4\Gamma^2} = \int_0^\infty d\omega \left[\frac{2\Gamma}{(\hbar\omega+\Delta)^2+4\Gamma^2} + \frac{2\Gamma}{(\hbar\omega-\Delta)^2+4\Gamma^2}\right] = \frac{\pi}{\hbar}, \tag{38}$$

one can easily obtain

$$\int_0^\infty d\omega\ \sigma_c(\omega) = \frac{e^2 t_\perp^2 N(0) d\pi}{\hbar^2}\left[1+\left(\frac{2t_\perp}{\Delta}\right)^2\right], \tag{39}$$

which states the ω-sum rule for the optical conductivity.

C. DC Resistivity

Using the result (37) in the limit of $\omega \to 0$, we obtain the c-axis DC resistivity

$$\rho_c(T) = [\sigma_c(\omega\to 0)]^{-1} \sim t_\perp^{-2}\Gamma\left[\left(\frac{t_\perp}{\Delta}\right)^2 + \frac{\Gamma^2}{\Delta^2+4\Gamma^2}\right]^{-1}. \tag{40}$$

The semiconductor-like upturn behavior at low temperature is obtained when the second term (interband transition) is dominant.

D. Thermal conductivity

Based on Wiedemann-Franz law and using (37) at $\omega = 0$ or directly from (40), one obtains the c-axis thermal conductivity for the plane-plane bilayer

$$K_c(T) \ \sim\ t_\perp^2\left[\left(\frac{t_\perp}{\Delta}\right)^2 + \frac{\Gamma^2}{\Delta^2+4\Gamma^2}\right]. \tag{41}$$

Once again, $K_c(T)$ will show strong depression at low temperature when the interband transition dominates.

VI. CASE OF TIGHT-BINDING BANDS

So far we have used the simplified band structures (4) and have tried to get simple analytic final results. These have required some approximations which we now wish to remove. We start with tight-binding bands with momentum $\mathbf{k}$ confined to the first Brillouin zone of the copper-oxide plane. We take

$$\xi_1 = -2t_1[\cos(k_x a)+\cos(k_y a) -2B\cos(k_x a)\cos(k_y a)] - \mu_1 \tag{42a}$$

and

$$\xi_2 = -2t_2\cos(k_y a) - \mu_2. \tag{42b}$$

For a model with $\{t_1, t_2, \mu_1, \mu_2, t_\perp\} = \{70, 100, -65, -175, 20\}$ in meV and $B = 0.45$, the corresponding Fermi surface contours are shown in Fig. 6. The dashed line are the unperturbed Fermi surface which have been chosen so that they do not cross. They are also the contours for the hybridized case with finite $t_\perp$ and $k_z = \frac{\pi}{d}$ in which case $t(k_z)$ in Eq. (5) is zero. The solid lines are the contours for $k_z = 0$ where $t(k_z)$ has its maximum value in (5). The area between dashed and solid curves gives the dispersion in the z-direction of the Fermi surface in the three-dimensional Brillouin zone. For this model band structure, we have evaluated (10) without further approximations (using a three-dimensional numerical routine over the Brillouin zone as in our previous paper [1]) and found results (see Fig. 2 in Ref. [1]) for the frequency dependence of the c-axis conductivity in qualitative agreement with our Fig. 1.

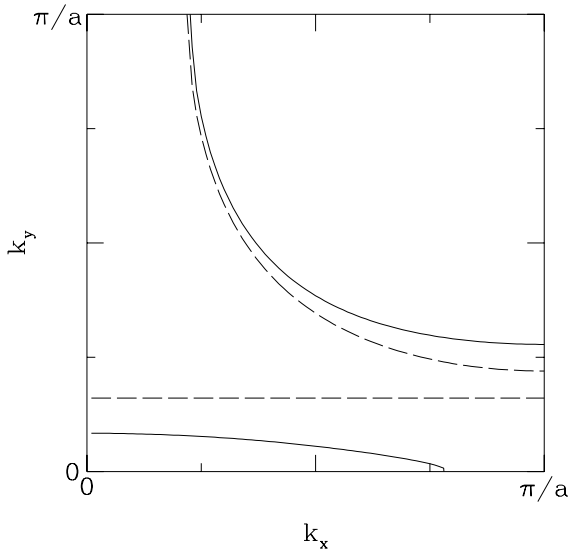

FIG. 6. The structure of the tight-binding bands given in Eq. (42). The parameters are $\{t_1, t_2, \mu_1, \mu_2, t_\perp\} = \{70, 100, -65, -175, 20\}$ meV and $B = 0.45$.

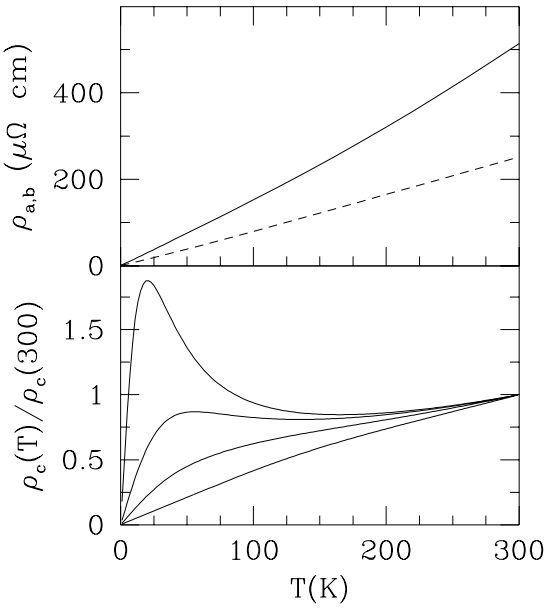

FIG. 7. Resistivity in the a (top frame, solid line), b (top frame, dashed line) and c (bottom frame) directions using the tight-binding bands. The a and b-axis resistivity are for $t_\perp = 2$meV and the c-axis resistivities are for $t_\perp = 2$, 5, 10, and 20 meV from top to bottom.

In Fig. 7, we show results for the DC resistivity. The top frame refers to the a- and b-directions, while the lower frame is for the c-axis resistivity $\rho_c(T)$ normalized to its value at $300K$. Four values of $t_\perp$ have been used for $\rho_c(T)$ namely $t_\perp = 2, 5, 10$ and 20 meV from the top to bottom. On comparing this frame with our previous Fig. 3, it is clear that there is no qualitative differences between the two models and use of the more realistic band structures has made only minor difference in our results for the DC resistivity. In the top frame of Fig. 7 ($t_\perp = 2$meV), the solid line is for the a-direction and the dashed line for the b-direction which is along the chain. While interband contributions have been included in the calculations with different values of $t_\perp$, this was found to make only small differences on the scale shown and so only a single curve is shown. For even higher values of $t_\perp$, larger differences should start showing up. In the case considered, the a-b plane resistivity $\rho_{ab}(T)$ is nearly linear in T but not quite. We note that our phenomenological assumption that the in-plane scattering rate $\Gamma(T)$ is linear in T leads directly to a linear dependence of $\rho_{ab}(T)$ vs. T in an infinite band model with constant density of states. The dashed line in the top frame of Fig. 7 is seen to be close to linear but this is not as true for the solid curve (along the a-direction) which shows two temperature scale – the second presumably related to the Van Hove singularity in the two-dimensional tight-binding band structures used here. There is also a small interband contribution further complicating the situation.

VII. CONCLUSIONS

In this paper we have derived approximate expressions for the frequency dependence of the c-axis conductivity for a bilayer cuprate based on simple free electron bands. The simplified results reproduced well our previous numerical results based on tight-binding bands [1]. The advantage of the present approach is that analytic results can be obtained in several important cases. Besides the AC infrared conductivity, we also give results for the DC resistivity, the optical conductivity sum rule and the thermal conductivity via the Wiedemann-Franz law. In the case of the c-axis resistivity, results of full numerical calculations based on tight-binding bands not presented before are also given and compared with the free electron case. In the discussion emphasis is placed on the role of the pseudogap which is identified as the *minimum* energy for interband transition possible in a given band structure.

ACKNOWLEDGMENTS

We thank Dwayne Branch for useful discussion. This work was supported by Natural Sciences and Engineering Research Council (NSERC) of Canada and Canadian Institute for Advanced Research (CIAR). One of the authors (W.A.) was supported in part by the Midwest Superconductivity Consortium through D.O.E. grant # DE-FG-02-90ER45427.

[1] W. A. Atkinson and J. P. Carbotte, Phys. Rev. B **55**, 3230 (1997).
[2] D. A. Bonn, P. Dosanjh, R. Liang, and W. N. Hardy, Phys. Rev. Lett. **68**, 2390 (1992).
[3] K. Zhang *et al.*, Phys. Rev. Lett. **73**, 2484 (1994).
[4] D. A. Bonn *et al.*, J. Phys. Chem. Solids. **56**, 1941 (1995).
[5] Y. Zha, S. L. Cooper, and D. Pines, Phys. Rev. B **53**, 8253 (1996).
[6] T. A. Friedmann, M. W. Rabin, J. Giapintzakis, J. P. Rice, and D. M. Ginsberg, Phys. Rev. B **42**, 6217 (1990).
[7] U. Welp, S. Fleshler, W. K. Kwok, J. Downey, Y. Fang, G. W. Crabtree, and J. Z. Liu, Phys. Rev. B **42**, 10189 (1990).
[8] Y. Iye, in *Physical Properties of High Temperature Superconductors III*, edited by D. M. Ginsberg (World Scientific, Singapore, 1992), p. 285.
[9] R. Gagnon, C. Lupien, and L. Taillefer, Phys. Rev. B **50**, 3458 (1994).
[10] H. Takei, H. Asaoka, Y. Iye, and H. Takeya, Jpn. J. Appl. Phys. **30**, L1102 (1991).
[11] Y. Iye *et al.*, Physica C **153-155**, 26 (1988).
[12] D. A. Brawner, Z. Z. Wang, and N. P. Ong, Phys. Rev. B **40**, 9329 (1989).

[13] K. Takenaka, K. Mizuhashi, H. Takagi, and S. Uchida, Phys. Rev. B **50**, 6534 (1994).
[14] G. D. Mahan, *Many-Particle Physics,* second edition (Plenum, New York, 1990), p. 777.
[15] W. A. Atkinson and J. P. Carbotte, Phys. Rev. B **52**, 10601 (1995).
[16] V. Ambegaokar and A. Griffin, Phys. Rev. **137**, A1151 (1965).
[17] D. J. Scalapino, in *Superconductivity Vol.1*, edited by R. D. Parks (Dekker, New York, 1969), p. 549.